Chinese Journal of Mechanical Engineering

ORIGINAL ARTICLE

Open Access

Configuration and Kinematics of a 3-DOF Generalized Spherical Parallel Mechanism for Ankle Rehabilitation

Jianjun Zhang[1,2*], Shuai Yang[1,2], Chenglei Liu[1,2], Xiaohui Wang[1,2] and Shijie Guo[1,2]

Abstract

The kinematic equivalent model of an existing ankle-rehabilitation robot is inconsistent with the anatomical structure of the human ankle, which influences the rehabilitation effect. Therefore, this study equates the human ankle to the UR model and proposes a novel three degrees of freedom (3-DOF) generalized spherical parallel mechanism for ankle rehabilitation. The parallel mechanism has two spherical centers corresponding to the rotation centers of tibiotalar and subtalar joints. Using screw theory, the mobility of the parallel mechanism, which meets the requirements of the human ankle, is analyzed. The inverse kinematics are presented, and singularities are identified based on the Jacobian matrix. The workspaces of the parallel mechanism are obtained through the search method and compared with the motion range of the human ankle, which shows that the parallel mechanism can meet the motion demand of ankle rehabilitation. Additionally, based on the motion-force transmissibility, the performance atlases are plotted in the parameter optimal design space, and the optimum parameter is obtained according to the demands of practical applications. The results show that the parallel mechanism can meet the motion requirements of ankle rehabilitation and has excellent kinematic performance in its rehabilitation range, which provides a theoretical basis for the prototype design and experimental verification.

Keywords Ankle rehabilitation, Parallel mechanism, Kinematic analysis, Parameter optimization

1 Introduction

The human ankle, which is one of the three joints of the lower extremity, is of fundamental importance for balance, support, and propulsion. Nevertheless, they are particularly susceptible to musculoskeletal and neurological injuries [1]. The traditional treatment of ankle injury highly depends on a one-by-one physical therapy by a doctor, which requires many human resources and heavy labor intensity. Moreover, the rehabilitation physician cannot objectively evaluate the rehabilitation status. Evidence suggests that without sufficient rehabilitation, 44% of people will experience problems in the future, and approximately 38% of people will have recurrent activity limitations that affect their functioning [2]. However, a machine-assisted treatment can collect real-time data during the entire rehabilitation process to provide targeted rehabilitation training for the patient, and it can also ensure the accuracy and repeatability of rehabilitation training.

Extensive research has been conducted on ankle-rehabilitation robots. Girone [3] developed a 6-DOF ankle-rehabilitation robot based on the Stewart platform; however, its structure was complex and difficult to control. Saglia et al. [4] proposed a 3-UPS/U (U, P, and S stand for universal, prismatic, and spherical pairs, respectively) parallel mechanism for ankle rehabilitation; however, the degrees of freedom of the mechanism was insufficient. Malosio et al. [5, 6]

*Correspondence:
Jianjun Zhang
zhjjun@hebut.edu.cn
[1] School of Mechanical Engineering, Hebei University of Technology, Tianjin 300401, China
[2] Key Laboratory of Robot Perception and Human-Machine Fusion, Tianjin 300401, China

designed an ankle-rehabilitation robot based on a 3-RRR (R stands for revolute pair) spherical mechanism. The robot had a remote rotation center, and the ankle center was located at the center of movement of the mechanism during rehabilitation. Li et al. [7–9] presented 3-RRS, 2-UPS/RRR, and 3-UPS/RRR parallel mechanisms for ankle rehabilitation. These three mechanisms equated an ankle to an S-pair, and all had a remote rotation center. Fang [10] proposed a rope-driven parallel mechanism for ankle rehabilitation. The mechanism also equated the ankle to an S-pair, which solved the problem of inertial impact caused by rigid rods. Bian et al. [11, 12] developed a biological fusion ankle-rehabilitation mechanism that uses the motion characteristics of the ankle to constrain the degrees of freedom of movement of the mechanism. Chen et al. [13] equated the ankle with a spatial RR model and proposed an ankle-rehabilitation mechanism based on the 3-UPU.

In summary, although the current ankle-rehabilitation robot meets basic rehabilitation training requirements, it still has certain limitations. Most ankle-rehabilitation robots equate the ankle and an S-pair [14] or a spatial RR model [15]. The ankle is one of the most complex joints of the human body. Its structural complexity and motion particularity prevent its axes of motion from intersecting at one point; however, there are multiple instantaneous rotation axes [16, 17]. The equivalence of the ankle to the S-pair or spatial RR model generates a human-machine interaction force, which makes the rehabilitation training effect unsatisfactory, and even causes secondary damage to patients. To improve the fitting accuracy of human-machine motion, this study equates the ankle with the UR model based on ankle anatomy and motion characteristics and proposes a novel 2-UPU/[RR][RRR]/PRPS generalized spherical parallel mechanism for ankle rehabilitation.

The remainder of this paper is organized as follows: In Section 2, the UR model is described with respect to the anatomical structure of the ankle. In Section 3, a parallel mechanism based on the UR model is proposed, the structure of the parallel mechanism is described in detail, and a systematic analysis of the parallel mechanism is performed, including the inverse kinematics, Jacobian matrix, singularity, and workspace. In Section 4, based on motion–force transmissibility, the parameters of the parallel mechanism are optimized. Finally, the conclusions are presented in Section 5.

2 Anatomical Structure and Equivalent Model of the Human Ankle

Research of the anatomical structure and motion forms of the ankle is the premise and key to the design of an ankle-rehabilitation mechanism, and it is also an important basis for evaluating the safety, man-machine coordinates, and comfort of ankle-rehabilitation mechanisms.

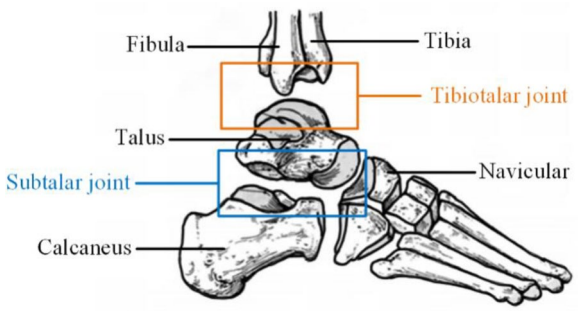

Figure 1 Anatomical structure of the ankle

2.1 Anatomical Structure of the Human Ankle

As shown in Figure 1, the ankle is a highly adaptive uniaxial joint that is mainly composed of the tibiotalar and subtalar joints [18]. The tibiotalar joint forms the junction between the distal tibia and fibula of the lower leg and talus, and the subtalar joint is between the talus and calcaneus. Both the tibiotalar and subtalar joints collectively bear the weight and movement of the lower extremity. The main motion forms of the ankle include dorsiflexion/plantarflexion, occurring in the sagittal plane; inversion/eversion, occurring in the transverse plane; and adduction/abduction, occurring in the frontal plane [19]. The axes of motion of the ankle are not fixed and have no confluence but change constantly with the ankle movement [18].

2.2 Equivalent Model of the Human Ankle

Currently, scholars in the field of ankle rehabilitation consider the spatial RR model or S-pair as the equivalent model of the ankle. The two rotation axes of the spatial RR model correspond to the rotation axes of the tibiotalar and subtalar joints of the ankle; however, they ignore the motion forms of the ankle. The S-pair considers the motion forms of the ankle and ignores the real structure of the ankle. Liu et al. [20] proposed a series of equivalent ankle models with respect to the physiological structure and motion characteristics of the ankle. According to the anatomical structure of the human ankle, the direction and position of the rotation axis of the tibiotalar joint change with its activities, whereas the rotation axis of the subtalar joint is relatively stable [21]. Therefore, this study adopts the UR model as the kinematic equivalent model of the human ankle, in which the tibiotalar joint is equivalent to the U-pair and the subtalar joint is equivalent to the R-pair. The distance from the geometric center of the U-pair to the R-pair is the size of the human talus, as shown in Figure 2.

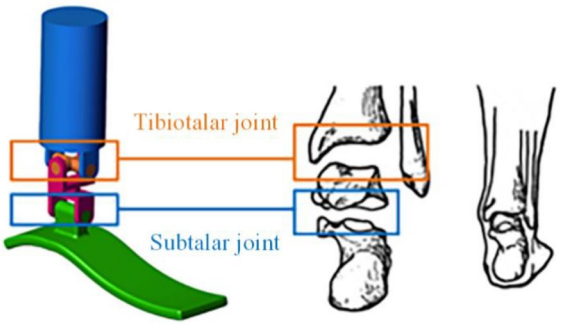

Figure 2 Equivalent model of the human ankle

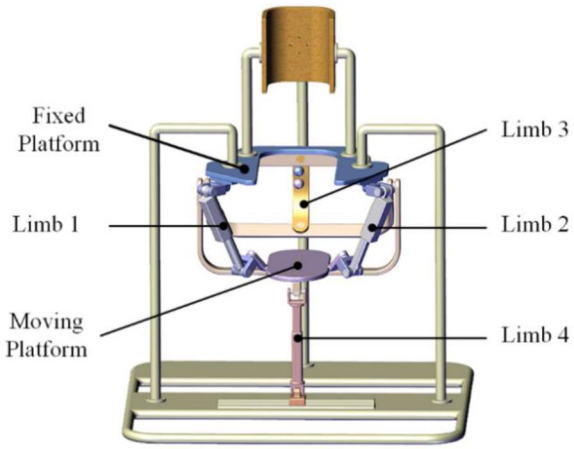

Figure 3 CAD model of the 2-UPU/[RR][RRR]/PRPS parallel mechanism for ankle rehabilitation

3 Ankle-Rehabilitation Mechanism

Owing to the limitation of the size of the human talus, it is difficult for the serial equivalent model to meet rehabilitation requirements. Therefore, a parallel mechanism was designed with respect to the motion forms of the serial equivalent model to improve the rehabilitation accuracy of the ankle.

3.1 Structure of the Ankle-Rehabilitation Mechanism

Figure 3 shows the structure of the 2-UPU/[RR][RRR]/PRPS parallel mechanism for ankle rehabilitation based on the UR-equivalent model. The parallel mechanism has two rotation centers, namely a fixed spherical center O, which is equivalent to the rotation center of the tibiotalar joint, and a moving spherical center O_1, which is equivalent to the rotation center of the subtalar joint. Point O is located at the intersection of the rotation axes on the fixed platform and point O_1 is located at the intersection point of the rotation axes on the moving platform. The line between points O and O_1 is called the 'double-centered line', and its length is equal to the size of the talus.

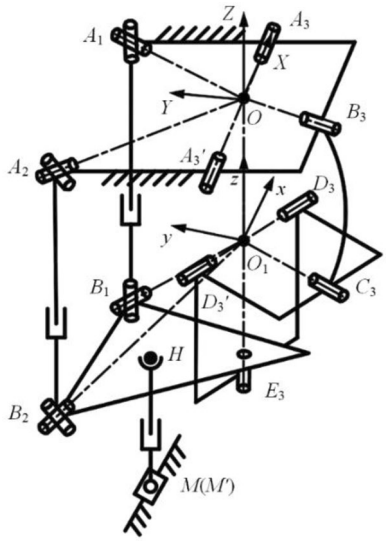

Figure 4 Schematic model of the 2-UPU/[RR][RRR]/PRPS parallel mechanism for ankle rehabilitation

The parallel mechanism has four limbs between the fixed and moving platforms. Limbs 1 and 2 are UPU limbs, and the rotation axes connected to the fixed platform are perpendicular to each other and intersect at point O. The rotation axes connected to the moving platform intersect at point O_1. The rotation axes connected to the P-pair are parallel to each other. Limb 3 is the [RR][RRR] limb, in which the first two rotation axes intersect at point O and the remaining rotation axes intersect at point O_1. Limb 4 is an unconstrained PRPS limb in which the axis of the R-pair coincides with the direction of the guide rail. The P-pairs of Limbs 1 and 2 and the slider of Limb 4 are the actuators.

As shown in Figure 4, point A_i (i=1, 2) is the center of the U-pair connected to the fixed platform in the ith limb. Point B_i (i=1, 2) is the center of the U-pair connected to the moving platform in the ith limb. Points A_3 and A_3' are the centers of the R-pairs connected to the fixed platform in Limb 3. Point E_3 is the center of the R-pair connected to the moving platform in Limb 3. Point H is the center of the S-pair in Limb 4. Point M is the center of the guide rail.

With point O as the origin of the coordinate system, the X-axis coincides with OA_3, the Z-axis is perpendicular to the fixed platform upward, and the Y-axis satisfies the right-hand rule; thus, the fixed coordinate system O-XYZ is established. Point O_1 is taken as the origin of the coordinates, the x-axis is parallel to the direction of B_2B_1, the z-axis is perpendicular to the platform moving upward, and the y-axis satisfies the right-hand rule; thus, the moving coordinate system O_1-xyz is established.

3.2 Degrees of Freedom

The DOF of the 2-UPU/[RR][RRR]/PRPS parallel mechanism for ankle rehabilitation was analyzed using screw theory [22]. In screw theory, a unit screw $\$$ is defined as

$$\$ = (\boldsymbol{s}\ \boldsymbol{s}_0) = (\boldsymbol{s}\ \boldsymbol{r} \times \boldsymbol{s} + h\boldsymbol{s}), \tag{1}$$

where $\boldsymbol{s}$ is the unit vector along the direction of the screw axis, $\boldsymbol{r}$ is the position vector of any point on the screw axis, and h is the pitch.

The motion screws of Limb 1 are given in the fixed coordinate system by

$$\begin{cases} \$_{11} = (\boldsymbol{s}_{OA_1}\ \boldsymbol{0}), \\ \$_{12} = (\boldsymbol{s}_{12}\ \boldsymbol{r}_{A_1} \times \boldsymbol{s}_{12}), \\ \$_{13} = (\boldsymbol{0}\ \boldsymbol{s}_{A_1B_1}), \\ \$_{14} = (\boldsymbol{s}_{12}\ \boldsymbol{r}_{B_1} \times \boldsymbol{s}_{12}), \\ \$_{15} = (\boldsymbol{s}_{O_1B_1}\ \boldsymbol{r}_{O_1} \times \boldsymbol{s}_{O_1B_1}), \end{cases} \tag{2}$$

where $\boldsymbol{s}_{OA1}$ is a unit vector along the direction of the first rotation axis of the U-pair in Limb 1 connected to the fixed platform; $\boldsymbol{s}_{12}$ is a unit vector along the direction of the second rotation axis of the U-pair in Limb 1 connected to the fixed platform; $\boldsymbol{r}_{A1}$ is the position vector of point A_1; $\boldsymbol{s}_{A1B1}$ is a unit vector along the direction of the P-pair in Limb 1; $\boldsymbol{r}_{B1}$ is the position vector of point B_1; $\boldsymbol{s}_{O1B1}$ is a unit vector along the direction of the first rotation axis of the U-pair in Limb 1 connected to the moving platform; and $\boldsymbol{r}_{O1}$ is the position vector of point O_1.

Then, by employing the reciprocal screw theory, the constraint screw of Limb 1 $\$_{C1}$ can be obtained as

$$\$_{C1} = (\boldsymbol{s}_{12}\ \boldsymbol{r}_{G_1} \times \boldsymbol{s}_{12}), \tag{3}$$

where G_1 is the intersection of the rotation axes in Limb 1 connected to the fixed and moving platforms, and $\boldsymbol{r}_{G1}$ is the position vector of point G_1.

The motion screws of Limb 2 can be expressed as

$$\begin{cases} \$_{21} = (\boldsymbol{s}_{OA_2}\ \boldsymbol{0}), \\ \$_{22} = (\boldsymbol{s}_{22}\ \boldsymbol{r}_{A_2} \times \boldsymbol{s}_{22}), \\ \$_{23} = (\boldsymbol{0}\ \boldsymbol{s}_{A_2B_2}), \\ \$_{24} = (\boldsymbol{s}_{22}\ \boldsymbol{r}_{B_2} \times \boldsymbol{s}_{22}), \\ \$_{25} = (\boldsymbol{s}_{O_1B_2}\ \boldsymbol{r}_{O_1} \times \boldsymbol{s}_{O_1B_2}), \end{cases} \tag{4}$$

where $\boldsymbol{s}_{OA2}$ is a unit vector along the direction of the first rotation axis of the U-pair in Limb 2 connected to the fixed platform; $\boldsymbol{s}_{22}$ is a unit vector along the direction of the second rotation axis of the U-pair in Limb 2 connected to the fixed platform; $\boldsymbol{r}_{A2}$ is the position vector of point A_2; $\boldsymbol{s}_{A2B2}$ is a unit vector along the direction of the P-pair in Limb 2; $\boldsymbol{r}_{B2}$ is the position vector of point B_2; and $\boldsymbol{s}_{O2B2}$ is a unit vector along the direction of the first rotation axis of the U-pair in Limb 2 connected to the moving platform.

In a similar approach, the constraint screw of Limb 2 $\$_{C2}$ can be obtained as

$$\$_{C2} = (\boldsymbol{s}_{22}\ \boldsymbol{r}_{G_2} \times \boldsymbol{s}_{22}), \tag{5}$$

where G_2 is the intersection of the rotation axes in Limb 2 connected to the fixed and moving platforms, and $\boldsymbol{r}_{G2}$ is the position vector of point G_2.

The motion screws of Limb 3 can be written as

$$\begin{cases} \$_{31} = (\boldsymbol{s}_{OA_3}\ \boldsymbol{0}), \\ \$_{32} = (\boldsymbol{s}_{OB_3}\ \boldsymbol{0}), \\ \$_{33} = (\boldsymbol{s}_{O_1C_3}\ \boldsymbol{r}_{O_1} \times \boldsymbol{s}_{O_1C_3}), \\ \$_{34} = (\boldsymbol{s}_{O_1D_3}\ \boldsymbol{r}_{O_1} \times \boldsymbol{s}_{O_1D_3}), \\ \$_{35} = (\boldsymbol{s}_{O_1E_3}\ \boldsymbol{r}_{O_1} \times \boldsymbol{s}_{O_1E_3}), \end{cases} \tag{6}$$

where $\boldsymbol{s}_{OA3}$ is a unit vector along the direction of the rotation axis of the R-pair in Limb 3 connected to the fixed platform; $\boldsymbol{s}_{OB3}$ is a unit vector along the direction of the rotation axis of the second R-pair in Limb 3; $\boldsymbol{s}_{O1C3}$ is a unit vector along the direction of the rotation axis of the third R-pair in Limb 3; $\boldsymbol{s}_{O1D3}$ is a unit vector along the direction of the rotation axis of the fourth R-pair in Limb 3; and $\boldsymbol{s}_{O1E3}$ is a unit vector along the direction of the rotation axis of the fifth R-pair in Limb 3.

The constraint screw of Limb 3 $\$_{C3}$ can be obtained as

$$\$_{C3} = (\boldsymbol{s}_{OO_1}\ \boldsymbol{0}), \tag{7}$$

where $\boldsymbol{s}_{OO1}$ is a unit vector along the direction of the 'double-centered line.

Limb 4 is a PRPS limb with 6-DOF and no constraint screw.

The motion and constraint screws of the UPU limb and the [RR][RRR] limb are shown in Figure 5. According to Eqs. (3), (5), and (7), the parallel mechanism has three linearly independent constraint forces that are arbitrarily distributed in space. Under the restriction of three constraint forces, the mechanism can realize 2-DOF motions of the moving spherical center O_1 on the spherical surface with the fixed spherical center O as the center and OO_1 as the radius, which can rotate around the moving spherical center O_1 with 1-DOF, which is consistent with the motion characteristics of the UR equivalent model. The DOF of the parallel mechanism can be obtained using the modified G-K formula [23]:

$$F = d(n - g - 1) + \sum_{i=1}^{g} f_i + \nu - \zeta = 6(13 - 15 - 1) + 21 - 0 = 3, \tag{8}$$

where F denotes the number of DOF, d denotes the rank of the parallel mechanism, n denotes the number of

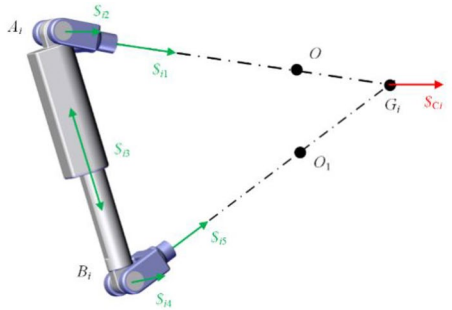

(a) The motion screws and constrain screw of the UPU limb

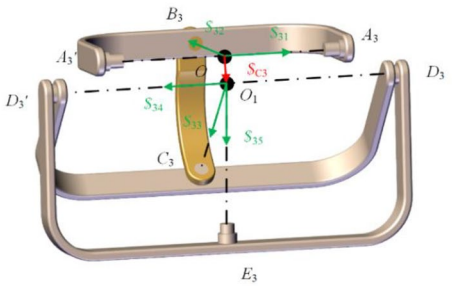

(b) Motion and constraint screws of the [RR][RRR] limb

Figure 5 Motion and constraint screws

components, g denotes the number of joints, f_i denotes the number of DOF for the ith joint, ν denotes the number of redundant constraints, and ζ denotes the number of isolated DOF.

3.3 Inverse Kinematic Analysis

Let the distance from point O to A_1 be l_{OA1}. Then, distance from point O to A_2 is denoted by l_{OA2}; the distance from point O_1 to B_1 is denoted by l_{O1B1}; the distance from point O_1 to B_2 is denoted by l_{O1B2}; the length of the 'double-centered line' is denoted by l; the distance from point O_1 to E_3 is denoted by l_{O1E3}; and the distance from point E_3 to H is denoted by l_{EH}. The angle between the axes of the U-pair connected to the moving platform and the moving platform is ϕ. l_{OA1}=l_{OA2}, l_{O1B1}=l_{O1B2}

The RPY angles α, β, and γ are used to represent the orientation of the moving platform relative to the fixed platform. The initial attitude of the moving coordinate system O_1-xyz is like that of the fixed coordinate system O-XYZ. First, O_1-xyz is rotated by α about the X-axis, then by β about the Y-axis, and finally by γ about the Z-axis. Thus, the rotation transformation matrix can be expressed as follows:

$$
{}^{O}_{O_1}\boldsymbol{R}(\alpha,\beta,\gamma) = \boldsymbol{R}(Z,\gamma)\boldsymbol{R}(Y,\beta)\boldsymbol{R}(X,\alpha)
$$

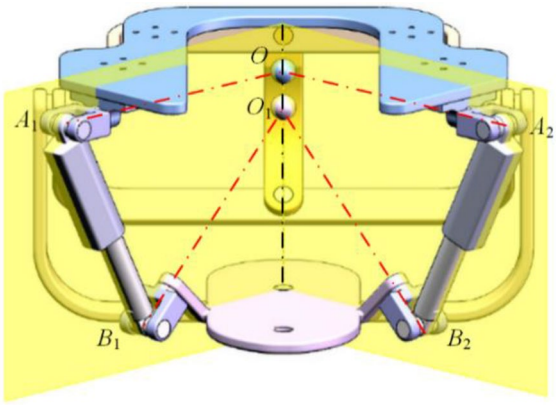

Figure 6 Schematic diagram of the 'double-centered line'

$$
= \begin{bmatrix} \mathrm{C}\beta\mathrm{C}\gamma & \mathrm{S}\alpha\mathrm{S}\beta\mathrm{C}\gamma - \mathrm{C}\alpha\mathrm{S}\gamma & \mathrm{C}\alpha\mathrm{S}\beta\mathrm{C}\gamma + \mathrm{S}\alpha\mathrm{S}\gamma \\ \mathrm{C}\beta\mathrm{S}\gamma & \mathrm{S}\alpha\mathrm{S}\beta\mathrm{S}\gamma + \mathrm{C}\alpha\mathrm{C}\gamma & \mathrm{C}\alpha\mathrm{S}\beta\mathrm{S}\gamma - \mathrm{S}\alpha\mathrm{C}\gamma \\ -\mathrm{S}\beta & \mathrm{S}\alpha\mathrm{C}\beta & \mathrm{C}\alpha\mathrm{C}\beta \end{bmatrix}, \tag{9}
$$

where C represents a cosine function and S represents a sine function.

Let the normal vectors of planes $OA_1B_1O_1$ and $OA_2B_2O_1$ be $\boldsymbol{n}_1$ and $\boldsymbol{n}_2$, respectively. Then,

$$
\boldsymbol{n}_1 : \begin{cases} \boldsymbol{n}_1 \cdot \boldsymbol{OA}_1 = 0, \\ \boldsymbol{n}_1 \cdot \mathbf{O}_1\boldsymbol{B}_1 = 0, \end{cases} \boldsymbol{n}_2 : \begin{cases} \boldsymbol{n}_2 \cdot \boldsymbol{OA}_2 = 0, \\ \boldsymbol{n}_2 \cdot \boldsymbol{O}_1\mathbf{B}_2 = 0. \end{cases} \tag{10}
$$

The intersection line of planes $OA_1B_1O_1$ and $OA_2B_2O_1$ is a straight line where the 'double-centered line' $\boldsymbol{OO}_1$ is located with respect to the structural characteristics of the parallel mechanism, as shown in Figure 6. Thus, the 'double-centered line' $\boldsymbol{OO}_1$ can be obtained as

$$
\boldsymbol{OO}_1 : \begin{cases} \boldsymbol{OO}_1 \cdot \boldsymbol{n}_1 = 0, \\ \boldsymbol{OO}_1 \cdot \boldsymbol{n}_2 = 0. \end{cases} \tag{11}
$$

The position vector of the origin (point O_1) of the moving coordinate system in the fixed coordinate system can be obtained as follows:

$$
\boldsymbol{O}_1 = \left(a_{O_1}, b_{O_1}, c_{O_1}\right)^{\mathrm{T}}. \tag{12}
$$

The position vectors of points B_1, B_2, and H in the moving coordinate system can be written as

$$
\begin{cases} \boldsymbol{b}_1 = (l_{O_1B_1}\mathrm{C}\varphi\mathrm{C}45^\circ, l_{O_1B_1}\mathrm{C}\varphi\mathrm{S}45^\circ, -l_{O_1B_1}\mathrm{S}\varphi)^{\mathrm{T}}, \\ \boldsymbol{b}_2 = (-l_{O_1B_2}\mathrm{C}\varphi\mathrm{C}45^\circ, l_{O_1B_2}\mathrm{C}\varphi\mathrm{C}45^\circ, -l_{O_1B_2}\mathrm{S}\varphi)^{\mathrm{T}}, \\ \boldsymbol{h} = (0, l_{EH}, -l_{O_1E_3})^{\mathrm{T}}. \end{cases} \tag{13}
$$

Through the transformation of the RPY angles, the position vectors of points B_1, B_2, and H in the fixed coordinate system can be expressed as:

$$\begin{cases} \boldsymbol{B}_1 = \boldsymbol{OO}_1 + {}^{O}_{O_1}\boldsymbol{R}(\alpha,\beta,\gamma)\boldsymbol{b}_1, \\ \boldsymbol{B}_2 = \boldsymbol{OO}_1 + {}^{O}_{O_1}\boldsymbol{R}(\alpha,\beta,\gamma)\boldsymbol{b}_2, \\ \boldsymbol{H} = \boldsymbol{OO}_1 + {}^{O}_{O_1}\boldsymbol{R}(\alpha,\beta,\gamma)\boldsymbol{h}. \end{cases} \tag{14}$$

Then, the lengths of Limbs 1 and 2, l_1 and l_2, are obtained as

$$\begin{cases} l_1 = |\boldsymbol{A}_1\boldsymbol{B}_1|, \\ l_2 = |\boldsymbol{A}_2\boldsymbol{B}_2|. \end{cases} \tag{15}$$

The angle between vector $\boldsymbol{MH}$ and the guide rail can be expressed as

$$\theta = \arccos\frac{\boldsymbol{MH}\cdot\boldsymbol{X}}{|\boldsymbol{MH}|}. \tag{16}$$

Then, the slider movement distance l_3 can be obtained as

$$l_3 = |\boldsymbol{MH}|\cos\theta. \tag{17}$$

3.4 Jacobian Matrix

The Jacobian matrix of a parallel mechanism, which represents the mapping between the joint input rates and moving platform output velocity, is an important tool for analyzing the kinematic performance and singularity of the parallel mechanism. Screw theory is used to establish the complete Jacobian matrix of the parallel mechanism.

The instantaneous screw of the moving platform [24] can be expressed as $\$_p = [\boldsymbol{w}^{\mathrm{T}}\ \boldsymbol{v}^{\mathrm{T}}]^{\mathrm{T}}$, which should be a linear combination of screws in Limb i (i=1–4).

$$\$_p = \dot{\theta}_{i1}\$_{i1}^{\mathrm{T}} + \dot{\theta}_{i2}\$_{i2}^{\mathrm{T}} + \dot{d}_{i3}\$_{i3}^{\mathrm{T}} + \dot{\theta}_{i4}\$_{i4}^{\mathrm{T}} + \dot{\theta}_{i5}\$_{i5}^{\mathrm{T}},\ i = 1, 2, \tag{18}$$

$$\$_p = \dot{\theta}_{i1}\$_{i1}^{\mathrm{T}} + \dot{\theta}_{i2}\$_{i2}^{\mathrm{T}} + \dot{\theta}_{i3}\$_{i3}^{\mathrm{T}} + \dot{\theta}_{i4}\$_{i4}^{\mathrm{T}} + \dot{\theta}_{i5}\$_{i5}^{\mathrm{T}},\ i = 3, \tag{19}$$

$$\begin{aligned} \$_p = {} & \dot{d}_{i1}\$_{i1}^{\mathrm{T}} + \dot{\theta}_{i2}\$_{i2}^{\mathrm{T}} + \dot{d}_{i3}\$_{i3}^{\mathrm{T}} \\ & + \dot{\theta}_{i4}\$_{i4}^{\mathrm{T}} + \dot{\theta}_{i5}\$_{5}^{\mathrm{T}} + \dot{\theta}_{i6}\$_{i6}^{\mathrm{T}},\ i = 4 \end{aligned} \tag{20}$$

where $\dot{\theta}_{ij}$ is the rotational angular velocity of the jth (j=1–6) joint in the ith limb; $\dot{d}_{ij}$ is the linear velocity of the prismatic in the ith limb; and $\$_{ij}$ is the unit screw of the jth joint in the ith limb.

As mentioned in Section 3.2, the parallel mechanism has three constraint screws. The constraint Jacobian matrix is obtained based on $\$_{Ci} \circ \$_p = 0$.

$$\boldsymbol{J}_C = \begin{bmatrix} \boldsymbol{r}_{G_1}\times\boldsymbol{s}_{12} & \boldsymbol{s}_{12} \\ \boldsymbol{r}_{G_2}\times\boldsymbol{s}_{22} & \boldsymbol{s}_{22} \\ \boldsymbol{0} & \boldsymbol{s}_{OO_1} \end{bmatrix}. \tag{21}$$

If we lock the actuated prismatic joint of the ith limb, a new unit-transmission screw $\$_{\mathrm{T}i}$ can be obtained, which represents the intermediate medium that transmits the power from the input to the output terminal [25].

$$\begin{cases} \$_{\mathrm{T1}} = (\boldsymbol{s}_{A_1B_1} \quad \boldsymbol{r}_{A_1}\times\boldsymbol{s}_{A_1B_1}), \\ \$_{\mathrm{T2}} = (\boldsymbol{s}_{A_2B_2} \quad \boldsymbol{r}_{A_2}\times\boldsymbol{s}_{A_2B_2}), \\ \$_{\mathrm{T3}} = (\boldsymbol{X} \quad \boldsymbol{r}_H\times\boldsymbol{X}). \end{cases} \tag{22}$$

Taking the reciprocity product on both sides of Eqs. (18) and (20) with $\$_{\mathrm{T}i}$ yields:

$$\begin{bmatrix} \boldsymbol{r}_{A_1}\times\boldsymbol{s}_{A_1B_1} & \boldsymbol{s}_{A_1B_1} \\ \boldsymbol{r}_{A_2}\times\boldsymbol{s}_{A_2B_2} & \boldsymbol{s}_{A_2B_2} \\ \boldsymbol{r}_H\times\boldsymbol{X} & \boldsymbol{X} \end{bmatrix}\$_p = \begin{bmatrix} \$_{\mathrm{T1}}\circ\$_{13} & 0 & 0 \\ 0 & \$_{\mathrm{T2}}\circ\$_{23} & 0 \\ 0 & 0 & \$_{\mathrm{T3}}\circ\$_{41} \end{bmatrix}\begin{bmatrix} \dot{d}_{13} \\ \dot{d}_{23} \\ \dot{d}_{41} \end{bmatrix}. \tag{23}$$

According to Eqs. (21) and (23), the velocity model of the 2-UPU/[RR][RRR]/PRPS parallel mechanism can be expressed as follows:

$$\boldsymbol{J}_p\$_p = \boldsymbol{J}_q\dot{\boldsymbol{q}}, \tag{24}$$

where

$$\boldsymbol{J}_p = \begin{bmatrix} \boldsymbol{r}_{G_1}\times\boldsymbol{s}_{12} & \boldsymbol{s}_{12} \\ \boldsymbol{r}_{G_2}\times\boldsymbol{s}_{22} & \boldsymbol{s}_{22} \\ \boldsymbol{0} & \boldsymbol{s}_{OO_1} \\ \boldsymbol{r}_{A_1}\times\boldsymbol{s}_{A_1B_1} & \boldsymbol{s}_{A_1B_1} \\ \boldsymbol{r}_{A_2}\times\boldsymbol{s}_{A_2B_2} & \boldsymbol{s}_{A_2B_2} \\ \boldsymbol{r}_H\times\boldsymbol{X} & \boldsymbol{X} \end{bmatrix},$$

$$\boldsymbol{J}_q = \mathrm{diag}(1,\ 1,\ 1, \$_{\mathrm{T1}}\circ\$_{13},\ \$_{\mathrm{T2}}\circ\$_{23},\ \$_{\mathrm{T3}}\circ\$_{41}),$$

$$\dot{\boldsymbol{q}} = [0,\ 0,\ 0,\ \dot{d}_{13},\ \dot{d}_{23},\ \dot{d}_{41}]^{\mathrm{T}},$$

$\boldsymbol{J}_p$ denotes the forward Jacobian matrix, $\boldsymbol{J}_q$ denotes the inverse Jacobian matrix, $\dot{\boldsymbol{q}}$ denotes the velocity of the input joint.

When the parallel mechanism is away from singularities, we have

$$\dot{\boldsymbol{q}} = \boldsymbol{J}_q^{-1}\boldsymbol{J}_p\$_p. \tag{25}$$

3.5 Singularity Analysis

When the parallel mechanism approaches the singularity configuration, the DOF is reduced or increased, which makes the parallel mechanism uncontrollable in certain directions. Based on the determinant of the Jacobian matrix, the singularity configuration of the parallel

mechanism is divided into three types [26, 27]. The first type, inverse singularity, occurs when $\det(\boldsymbol{J}_q) = 0$; the second type, forward kinematic singularity, occurs when $\det(\boldsymbol{J}_p) = 0$; and the third type, called combined singularity, occurs when $\det(\boldsymbol{J}_q) = 0$ and $\det(\boldsymbol{J}_p) = 0$. Because the human subtalar joint is always below the tibiotalar joint, this study considers the singularity of the workspace when the moving spherical center is lower than the fixed spherical center.

3.5.1 Inverse Singularity

Because matrix $\boldsymbol{J}_q$ is a diagonal matrix, inverse singularity occurs whenever any of the diagonal elements becomes zero. Moreover, all actuators of the parallel mechanism are prismatic pairs, and the direction of the real unit of $\$_{Ti}$ is consistent with the direction of the ith actuator. According to the reciprocity product theory, $\$_{T1} \circ \$_{13}$, $\$_{T2} \circ \$_{23}$ and $\$_{T3} \circ \$_{41}$ are always equal to one. Therefore, the parallel mechanism does not exhibit inverse singularity.

3.5.2 Forward Kinematic Singularity

Matrix $\boldsymbol{J}_p$ consists of three zero-pitch constraint screws and three zero-pitch transmission force screws. A zero-pitch screw can be represented as a line; therefore, the linear dependency among the screws becomes equivalent to the dependency between the lines they represent. Therefore, the forward kinematic singularity can be identified using the Grassmann line theory [28].

The three constraint forces provided by the four limbs to the moving platform are not always in the same plane as the change in the parallel mechanism configuration or position of the moving platform. According to the Grassmann line theory, the rank of the matrix composed of three constraint screws is always equal to three. Therefore, the condition for the forward kinematic singularity is that the rank of matrix $\boldsymbol{J}_p$ should be 3–5.

(1) The rank of matrix $\boldsymbol{J}_p$ is three, and there are three possible cases.

Case 1: The union of two flat pencils with a line in common but lying in distinct planes and with distinct centers. Because the three constraint screws are not always in the same plane, $\$_{C1}$ is perpendicular to $\$_{T1}$, $\$_{C2}$ is perpendicular to $\$_{T2}$, and the 'double-centered line' $\boldsymbol{OO}_1$ with $\boldsymbol{A}_1\boldsymbol{B}_1$ and $\boldsymbol{A}_2\boldsymbol{B}_2$ can never constitute a plane. Therefore, this case does not occur in the parallel mechanism.

Case 2: All lines pass through a point but are not coplanar. This case does not exist because the three transmission-force screws are consistent with the direction of the actuators, and the three constraint screws do not meet at one point.

Case 3: All lines are in a plane but do not constitute a planar pencil of lines. Because the three constraint screws are not always in the same plane, this case does not exist.

(2) Matrix $\boldsymbol{J}_p$ is ranked forth, and there are three possible cases.

Case 1: All lines in a plane pass through one point on that plane. According to the structure of the parallel mechanism, only three transmission-force screws may be in the same plane, but the three constraint screws never meet at one point, so this case does not exist.

Case 2: A one-parameter family of flat pencils, with one line in common and forming a variety. According to the structure of the parallel mechanism, $\$_{C1}$ is perpendicular to $\$_{T1}$ and is a non-coplanar straight line with $\$_{C3}$, $\$_{T2}$, and $\$_{T3}$. In the same way, $\$_{C2}$ is perpendicular to $\$_{T2}$, and is a non-coplanar straight line with $\$_{C3}$, $\$_{T1}$ and $\$_{T3}$. Moreover, $\$_{C1}$ and $\$_{C2}$ can only form a plane at the initial position. At this position, $\$_{T1}$ and $\$_{T2}$ can form a plane, but $\$_{T3}$ and $\$_{C3}$ cannot form a plane. Therefore, this case does not exist.

Case 3: All lines are concurrent with two skewed lines. According to the analysis of Case 2, this case does not exist.

(3) The rank of the matrix $\boldsymbol{J}_p$ is five, and there is one possible case: all the lines intersect one line. Because any one of these six lines has at least one set of non-coplanar lines, this case does not exist.

Through the above analysis, the parallel mechanism has no forward kinematic singularity.

3.5.3 Combined Singularity

A combined singularity occurs when forward and inverse kinematic singularities occur simultaneously. Because there is no inverse singularity or forward kinematic singularity in the parallel mechanism, it has no combined singularity.

3.6 Workspace

The workspace is a necessary condition for measuring whether the parallel mechanism can meet the rehabilitation requirements of the human ankle. In this study, the orientational workspace, moving spherical center, and moving platform workspace of the parallel mechanism for ankle rehabilitation were solved. The structural parameters of the parallel mechanism are presented in Table 1.

Under the condition that the moving distances of the P-pairs in Limbs 1 and 2 are limited to ±80 mm and

Table 1 The structural parameters of the parallel mechanism

Parameter	Value
l_{OA} (mm)	275
l_{O1B} (mm)	180
l (mm)	30
l_{E3H} (mm)	120
φ (°)	45

the rotation range of the U-pair is ±45°, the workspaces of the parallel mechanism are solved using the search method with the help of MATLAB. The results are shown in Figure 7. According to Ref. [29], the motion ranges of the human ankle and the parallel mechanism are listed in Table 2.

From the data in Table 2, the workspace of the parallel mechanism fully meets the motion range requirements of the human ankle. Therefore, a parallel mechanism for ankle rehabilitation can complete the rehabilitation exercises of the ankle.

4 Performance Analysis and Optimization

Currently, the performance evaluation indices applied to parallel mechanisms mainly include the condition number of the Jacobian matrix [30], dexterity [31], and motion/force transmissibility [32]. Based on screw theory, the motion–force transmissibility reflects the transmission efficiency of the motion and force of the parallel mechanism from the input to output. In this study, the motion/force transmissibility was used as the evaluation standard of the kinematic performance of the ankle-rehabilitation parallel mechanism, and the parameters were optimized based on this index.

4.1 Motion/Force Transmissibility

Motion–force transmissibility can be divided into the input and output transmissibility with respect to the transfer of objects between the input and output of the parallel mechanism. The input and output transmissibility of a single limb of the parallel mechanism can be expressed as:

$$\lambda_i = \frac{\left|\$_{\mathrm{T}i} \circ \$_{\mathrm{I}i}\right|}{\left|\$_{\mathrm{T}i} \circ \$_{\mathrm{I}i}\right|_{\max}}, \tag{26}$$

$$\eta_i = \frac{\left|\$_{\mathrm{T}i} \circ \$_{\mathrm{O}i}\right|}{\left|\$_{\mathrm{T}i} \circ \$_{\mathrm{O}i}\right|_{\max}}, \tag{27}$$

where λ_i denotes the input transmissibility, η_i denotes the output transmissibility, $\$_{\mathrm{I}i}$ denotes the input screw of the ith driving limb, $\$_{\mathrm{T}i}$ denotes the transmission-force screw of the ith driving limb, and $\$_{\mathrm{O}i}$ denotes the output screw of the ith actuated limb. Both λ_i and η_i were within the range of [0, 1].

To ensure that each limb has excellent input and output transmissibility, the local transmission index (LTI) [33] of the parallel mechanism is defined as

$$\Gamma = \min\{\lambda_i, \eta_i\}, \tag{28}$$

where Γ is a dimensionless index, independent of the coordinate system. The closer Γ is to one, the better the motion-force transmissibility of the parallel mechanism. The closer Γ is to zero, the closer the parallel mechanism is to singularity.

Furthermore, if any two actuated prismatic joints are locked and only the actuated prismatic joint of the ith limb is retained, then only the motion from the ith actuated prismatic joint can be transmitted to the moving platform under the action of the ith transmission force. In this situation, the parallel mechanism becomes a 1-DOF mechanism and the unit instantaneous screw of the moving platform can be expressed by the unit output screw $\$_{\mathrm{O}i}$. Therefore, according to the reciprocity of the motion and force screws, the unit output screw $\$_{\mathrm{O}i}$ can be obtained as follows:

$$\begin{cases} \$_{\mathrm{T}j} \circ \$_{\mathrm{O}i} = 0, \\ \$_{\mathrm{C}j} \circ \$_{\mathrm{O}i} = 0, \end{cases} \quad i \neq j. \tag{29}$$

The LTI of the parallel mechanism can be obtained by substituting the output motion screws into Eqs. (26)–(28). The distribution diagrams of the LTI of the parallel mechanisms in pure dorsiflexion/plantarflexion (α=0°), inversion/eversion (β=0°), and adduction/abduction (γ=0°) are illustrated in Figure 8(a)–(c), respectively. It can be observed from the figures that the LTI of the parallel mechanism in the central area of the workspace is greater than 0.7, and its value decreases progressively as it leans on the boundary of the workspace. There is no Γ=0 position in the target workspace, indicating that the parallel mechanism does not have singularity in the workspace.

4.2 Parameter Optimization

However, the LTI can only reflect the motion–force transmissibility of the parallel mechanism in a particular configuration but not in the entire workspace. Therefore, the global motion–force transmissibility, ζ, was introduced. When $\Gamma \geq 0.7$, the configuration sets of the parallel mechanism are defined as the high-quality transmission workspace [34]. The ratio of the high-quality transmission workspace to the entire workspace is the global motion-force transmissibility:

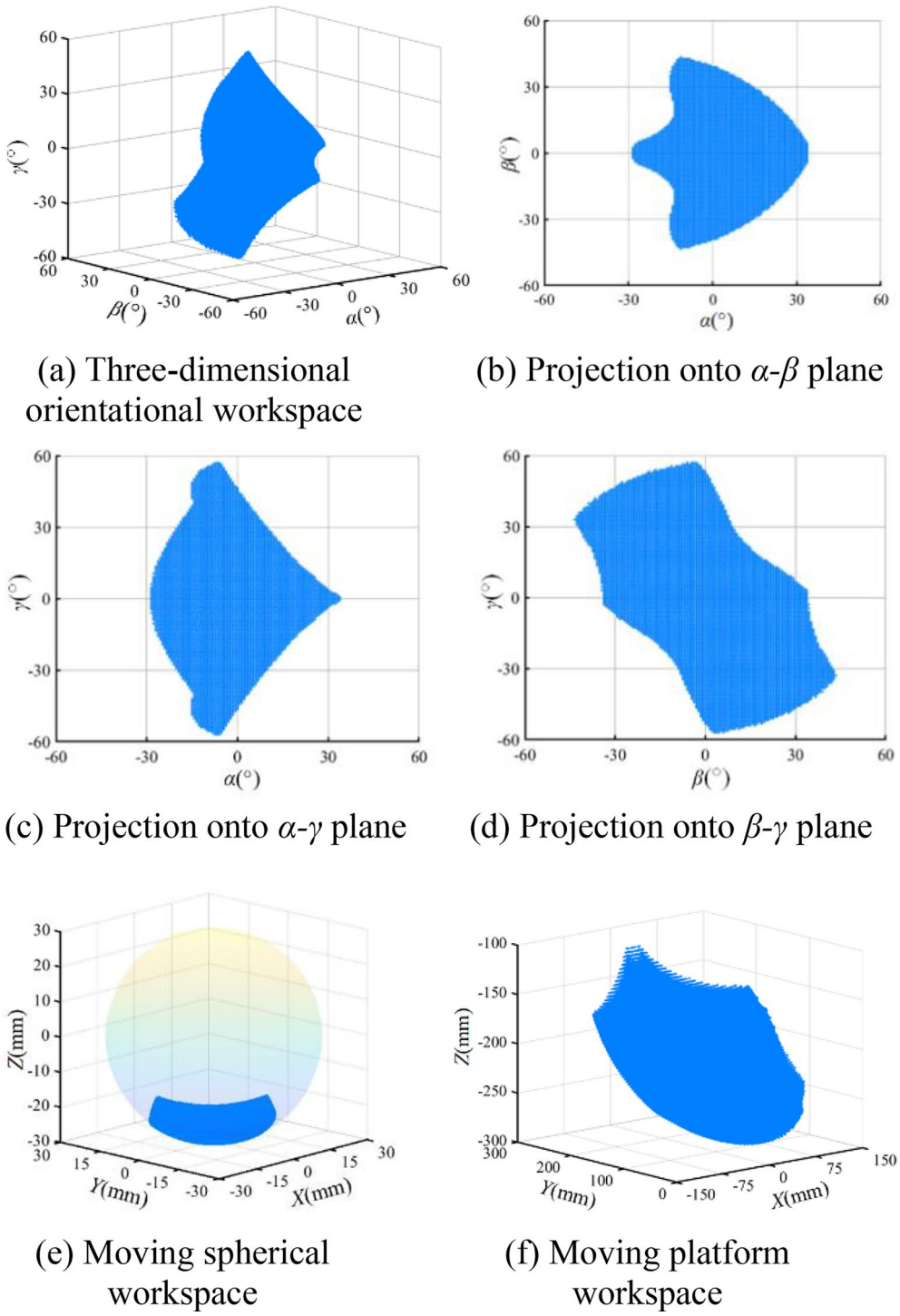

Figure 7 Workspaces of 2-UPU/[RR][RRR]/PRPS

$$\zeta=\frac{\int_{SG}\mathrm{d}W}{\int_{S}\mathrm{d}W}, \tag{30}$$

where W is the entire workspace, SG is the volume of the high-quality transfer workspace, S is the volume of the entire workspace, and ζ is within the range of [0, 1]. The

Table 2 Motion range of the human ankle and the parallel mechanism

Movement type	Motion range of human ankle (°) [29]	Motion range of parallel mechanism (°)
Dorsiflexion	20.3—29.8	34
Plantarflexion	37.6—45.7	51
Inversion	14.5—22.0	45
Eversion	10.0—17.0	45
Adduction	22.0—36.0	76
Abduction	15.4—25.9	76

closer ζ is to one, the better is the kinematic performance of the parallel mechanism.

By substituting the structural parameters in the previous section into Eq. (30), the global motion–force transmissibility of the parallel mechanism was 0.33. This shows that the motion-force transmissibility of the parallel mechanism is not excellent under such structural parameters. Therefore, further optimization is required.

In this study, the optimization method proposed in Ref. [35] is used to optimize three structural parameters: the distance from point O to point A_i, l_{OA}, distance from point O_1 to B_i, ; and distance from point H to E_3, l_{EH}. First, the structural parameters are dimensionless and are treated as follows:

$$\begin{cases} D = \dfrac{l_{OA} + l_{O_1B} + l_{EH}}{3}, \\ r_1 = \dfrac{l_{OA}}{D}, r_2 = \dfrac{l_{O_1B}}{D}, r_3 = \dfrac{l_{EH}}{D}, \end{cases} \tag{31}$$

where D is the normalized factor and r_i is the dimensionless parameter of the three optimization parameters.

Considering the interference between the various components of the parallel mechanism and stroke of the push link, the dimensionless parameters should satisfy the following conditions:

$$\begin{cases} r_1 + r_2 + r_3 = 3, \\ r_3 \le r_2, \\ r_2 \le r_1. \end{cases} \tag{32}$$

According to Eq. (32), the parameter-optimization region of the parallel mechanism can be obtained, as shown in Figure 9(a). It is projected onto the s-t coordinates to obtain Figure 9(b); therefore, the three-dimensional space is reduced to a two-dimensional space to reduce the optimization parameters. The mapping relationship is obtained as follows:

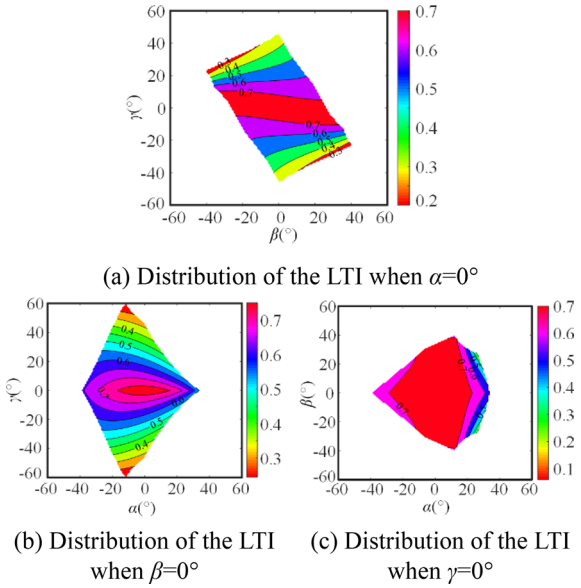

(a) Distribution of the LTI when α=0°

(b) Distribution of the LTI when β=0°

(c) Distribution of the LTI when γ=0°

Figure 8 Distribution of the LTI for 2-UPU/[RR][RRR]/PRPS

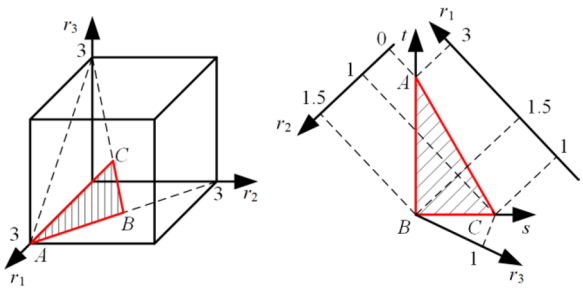

(a) Spatial expression (b) Planar expression

Figure 9 Parameter design space of 2-UPU/[RR][RRR]/PRPS

$$\begin{cases} r_1 = -\dfrac{\sqrt{6}}{6}s + \dfrac{\sqrt{2}}{2}t + \dfrac{3}{2}, \\ r_2 = -\dfrac{\sqrt{6}}{6}s - \dfrac{\sqrt{2}}{2}t + \dfrac{3}{2}, \\ r_3 = \dfrac{\sqrt{6}}{3}s. \end{cases} \tag{33}$$

MATLAB was used to conduct an iterative search over the entire s-t region, as shown in Figure 9(b). The global motion–force transmissibility of the corresponding size was calculated, and performance atlases were plotted, as shown in Figure 10. The figure shows that the global motion–force transmissibility of the parallel mechanism in the range of $0.6 \le s \le 1.22$ and $0 \le t \le 0.2$ is greater than 0.5. This shows that the parameters

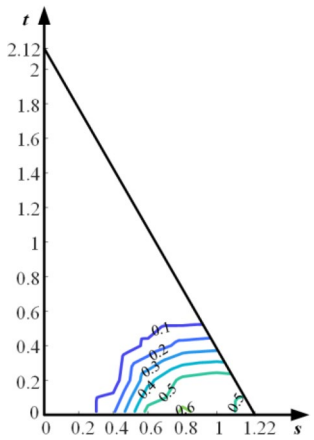

Figure 10 Distribution of LTI in the parameters design

of the parallel mechanism have an excellent kinematic performance within this range.

Considering the rationality of the layout between the links of the parallel mechanism and workspace, s=0.8, t=0.2, and D=200 mm were selected. The corresponding mechanism parameters are $l_{OA}=D\cdot r_1\approx 255$ mm, $l_{O1B}=D\cdot r_2\approx 215$ mm, and $l_{EH}=D\cdot r_3\approx 131$ mm. Then, the parameters are substituted into Eqs. (26)–(28), and the distribution diagrams of the LTI are shown in Figure 11.

By comparing the distribution diagrams of the LTI of the parallel mechanism before optimization, the area of the high-quality transfer workspace after optimization was significantly increased, and the global motion–force transmissibility of the parallel mechanism after optimization reached 0.59. This indicates that the kinematic performance of the optimized parallel mechanism was significantly improved.

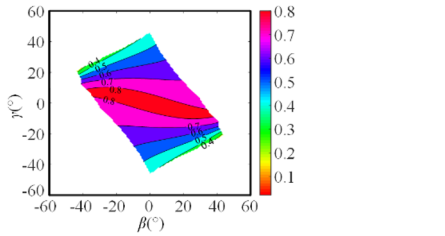

(a) Distribution of the LTI for the optimized mechanism when α=0°

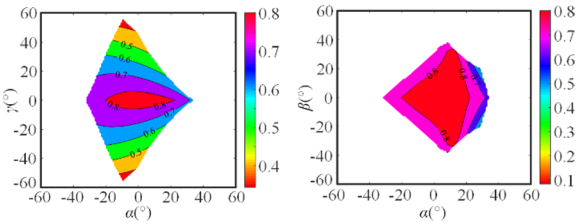

(b) Distribution of the LTI for the optimized mechanism when β=0°

(c) Distribution of the LTI for the optimized mechanism when γ=0°

Figure 11 Distribution of the LTI for the optimized parallel mechanism

5 Conclusions

(1) Based on the anatomical structure and motion characteristics of the human ankle, the UR equivalent model was selected, and a novel 2-UPU/[RR][RRR]/PRPS generalized spherical parallel mechanism for ankle rehabilitation was presented. Screw theory analysis revealed that the parallel mechanism has three rotational DOFs that satisfy the demand for ankle rehabilitation.

(2) The inverse kinematics of the parallel mechanism were analyzed using an analytical method. According to screw theory, a complete Jacobian matrix was established, and the singularity was investigated based on inverse singularity, forward kinematic singularity, and combined singularity, indicating that the parallel mechanism has no singularity. Additionally, the workspaces were solved, and they showed that the parallel mechanism satisfied the motion range of the human ankle.

(3) By considering the motion–force transmissibility, the global motion–force transmissibility was used as the performance evaluation criterion in this study, and the performance atlases were plotted in the parameter-optimal design space. Subsequently, according to the demands of practical applications, the optimum region was obtained. The results show that the ratio of the high-quality transmission workspace reached 0.59, which indicates that the parallel mechanism has excellent kinematic performance in the ankle-rehabilitation motion range.

Acknowledgements
Not applicable.

Authors' Contributions
JZ was in charge of the whole research; SY wrote the manuscript; CL assisted with the analysis and validation. The remaining discussed and read the manuscript. All authors read and approved the final manuscript.

Funding
Supported by National Natural Science Foundation of China (Grant No. 52075145), S&T Program of Hebei Province of China (Grant Nos. 20281805Z, E2020103001), and Central Government Guides Basic Research Projects of Local Science and Technology Development Funds of China (Grant No. 206Z1801G).

Competing Interests
The authors declare no competing financial interests.

Received: 12 August 2021 Revised: 5 February 2024 Accepted: 5 February 2024
Published online: 12 March 2024

References

[1] M M Zhang, T C Davies, S N Xie. Effectiveness of robot-assisted therapy on ankle rehabilitation-a systematic review. *Journal of NeuroEngineering and Rehabilitation*, 2013, 10(1): 30.
[2] M J Dong, Y Zhou, J F Li, et al. State of the art in parallel ankle rehabilitation robot: a systematic review. *Journal of NeuroEngineering and Rehabilitation*, 2021, 18(1): 52.
[3] M Girone, G Burzit, M Bouzit, et al. A stewart platform-based system for ankle tele-rehabilitation. *Autonomous Robots*, 2001, 10(2): 203–212.
[4] J A Saglia, N G Tsagarakis, J S Dai, et al. Control strategies for patient-assisted training using the ankle rehabilitation robot (ARBOT). *IEEE/ASME Transactions on Mechatronics*, 2013, 18(6): 1799–1808.
[5] M Malosio, S P Negri, N Pedrocchi, et al. A spherical parallel three degrees-of-freedom robot for ankle-foot neuro-rehabilitation. *2012 Annual International Conference of the IEEE Engineering in Medicine and Biology Society*, San Diego, USA, August 28–September 1, 2012: 3356–3359.
[6] M Malosio, M Caimmi, M Ometto, et al. Ergonomics and kinematic compatibility of PKankle, a fully-parallel spherical robot for ankle-foot rehabilitation. *5th IEEE RAS/EMBS International Conference on Biomedical Robotics and Biomechatronics(BioRob)*, San Diego, USA, August 12–15 2014: 497–503.
[7] D S Li, J F Li, S Wang, et al. Analysis on 3-RRS mechanism for ankle rehabilitation anf its kinematics. *Machinery Design & Manufacture*, 2015, 8: 4–8. (in Chinese)
[8] J F Li, S C Li, C J Tao, et al. Parallel 2-UPS/RRR ankle rehabilitation mechanism and kinematic performance analysis. *Robot*, 2016, 38(2): 144–153. (in Chinese)
[9] J F Li, C H Xu, C J Tao, et al. A parallel ankle rehabilitation mechanism and its performance analysis based on 3-UPS/RRR. *Acta Automatica Sinica*, 2016, 42(12): 1794–1807. (in Chinese)
[10] R T Yu, Y F Fang, S Guo, et al. Design and kinematic performance analysis of a cable-drive parallel mechanism for ankle rehabilitation. *Robot*, 2015, 37(1): 53–62. (in Chinese)
[11] H Bian, T S Zhao, X B Tian, et al. Biological fusion rehabilitation institution and its application. *Robot*, 2010, 32(4): 470–477. (in Chinese)
[12] H Bian, Y H Liu, T S Zhao, et al. Mechanism and kinematics of parallel 2-RRR/UPRR ankle rehabilitation robot. *Robot*, 2010, 32(1): 6–12. (in Chinese)
[13] Z M Chen, T Yi, H Pan, et al. A 3-DOF parallel ankle rehabilitation mechanism. *Journal of Mechanical Engineering*, 2020, 56(21): 70–78. (in Chinese)
[14] C Z Wang, Y F Fang, S Guo, et al. Design and kinematic analysis of redundantly actuated parallel mechanism for ankle rehabilitation. *Robotica*, 2015, 33(2): 366–384.
[15] J Dui, G E Johnson. A kinematic model of the human ankle. *Journal of Biomedical Engineering*, 1985, 7(2): 137–143.
[16] S V S Jan, P Salvia, V Feipet, et al. In vivo registration of both electrogoniometry and medical imaging: development and application on the ankle joint complex. *IEEE Transactions on Biomedical Engineering*, 2006, 53(4): 759–762.
[17] S Canton, W Anderst, M Hogan. In vivo ankle kinematics revealed through biplane radiography: current concepts, recent literature, and future directions. *Current Reviews in Musculoskeletal Medicine*, 2020, 13(1): 77–85.
[18] B Y Mao, Q J Pang, K R Dai. *Surgery of the total ankle*. Beijing: People's Military Medical Press, 2015. (in Chinese)
[19] C L Brockett, G J Chapman. Biomechanics of the ankle. *Orthopaedics and Trauma*, 2016, 30(3): 232–238
[20] C L Liu, J J Zhang, K C Qi, et al. Type synthesis of generalized spherical parallel mechanisms for ankle rehabilitation. *Journal of Mechanical Engineering*, 2020, 56(19): 79–91. (in Chinese)
[21] X F Gong, Y Wu, M Y Wang. Functional anatomy and biomechanics of the ankle. *Chinese Journal of Surgery*, 2010, 48(9): 670-674.
[22] S H Li, Z Huang. Comparative analysis of characteristics of the coupled and decoupled parallel mechanisms. *Chinese Journal of Mechanical Engineering*, 2010, 23(4): 468–476.
[23] Z Huang, J F Liu, Y W Li. *On the DOF of mechanism — Searching for the general formula of DOF for 150 years*. Beijing: Science Press, 2011. (in Chinese)
[24] W Ye, X X Chai, K T Zhang. Kinematic modeling and optimization of a new reconfigurable parallel mechanism. *Mechanism and Machine Theory*, 2020, 149: 103850.
[25] M J Song, S Guo, X Y Wang, et al. Dynamic analysis and performance verification of a novel hip prosthetic mechanism. *Chinese Journal of Mechanical Engineering*, 2020, 33: 17.
[26] L Kang, S M Oh, W Kim, et al. Design of a new gravity balanced parallel mechanism with Schönflies motion. *Proceedings of the Institution of Mechanical Engineers, Part C: Journal of Mechanical Engineering Science*, 2015, 230(17): 3111–3134.
[27] S M Kim, B J Yi, W Kim. Forward kinematic singularity avoiding design of a Schönflies motion generator by asymmetric attachment of sun-chains. *International Journal of Control, Automation and Systems*, 2013, 11(1): 116-126.
[28] J P Merlet. Singular configurations of parallel manipulators and Grassmann geometry. *The International Journal of Robotics Research*, 1989, 8(5): 45–56.
[29] S Siegler, J Chen, C D Schneck. The three-dimensional kinematics and flexibility characteristics of the human ankle and subtalar joints–Part I: kinematics. *Journal of Biomechanical Engineering*, 1988, 110(4): 364–373.
[30] C Gosselin, J Angeles. The optimum kinematic design of a spherical three-degree-of-freedom parallel manipulator. *Journal of Mechanical Design*, 1989, 111(2): 202–207.
[31] R S Stoughton, T Arai. A modified Stewart platform manipulator with improved dexterity. *IEEE Transactions on Robotics and Automation*, 1993, 9(2): 166–173.
[32] J S Wang, C Wu, X J Jun. Performance evaluation of parallel manipulators: Motion/force transmissibility and its index. *Mechanism and Machine Theory*, 2010, 45(10): 1462–1476.
[33] Q Z Meng, F G Xie, X J Liu, et al. An evaluation approach for motion-force interaction performance of parallel manipulators with closed-loop passive limbs. *Mechanism and Machine Theory*, 2020, 149: 103844.
[34] X J Liu, F G Xie, J S Wang. *Fundamental of parallel robotic mechanisms*. Beijing: Higher Education Press, 2018. (in Chinese)
[35] C Wu, X J Liu, L P Wang, et al. Optimal design of spherical 5R parallel manipulators considering the motion/force transmissibility. *Journal of Mechanical Design*, 2010, 132(3): 031002.

Jianjun Zhang Born in 1971, is currently a professor and a PhD candidate supervisor at *Key Laboratory of Robot Perception and Human-Machine Fusion, Hebei University of Technology, China*. He received his PhD degree from *Beijing University of Aeronautics and Astronautics, China*, in 2004. His research interests include the robotic mechanics, exoskeleton robot, and rehabilitation robot.

Shuai Yang Born in 1996, is currently a master candidate at *Key Laboratory of Robot Perception and Human-Machine Fusion, Hebei University of Technology, China*. His research interests include parallel mechanisms and rehabilitation robot.

Chenglei Liu Born in 1995, is currently a PhD candidate at *Key Laboratory of Robot Perception and Human-Machine Fusion, Hebei University of Technology, China*. His research interests include parallel mechanism and rehabilitation robot.

Xiaohui Wang Born in 1970, is currently an associated professor at *Key Laboratory of Robot Perception and Human-Machine Fusion, Hebei University of Technology, China*. Her research interests include robotic mechanics.

Shijie Guo Born in 1963, is currently a professor and a PhD candidate supervisor at *Key Laboratory of Robot Perception and Human-Machine Fusion, Hebei University of Technology, China*. He received his PhD degree from *Tokyo Institute of Technology, Japan*, in 1992. His research interests include the man-machine integration system, nursing robot, and unbound physiological information monitoring system.